 CMES, vol.6, no.4, pp.397-408, 2004

Analysis of Wrinkling Behavior of Anisotropic Membrane

K. Woo[1], H. Igawa[2], and C.H. Jenkins[3]

Abstract: This paper presents the development and evaluation of a wrinkling analysis procedure for anisotropic membranes. The procedure is based on a penalty-parameter modified material model and a non-linear root finding to simulate the uni-axial stress state. The procedure was implemented in the ABAQUS finite element code as a user subroutine, and then applied to annular and square membranes. The wrinkle problems were also solved by shell element post-buckling analysis and the results were compared. The effect of anisotropy and unsymmetric loading on the wrinkling behavior was investigated.

keyword: Membrane, wrinkle, anisotropic, penalty-parameter.

1 Introduction

There has been growing interest in the application of membrane materials to gossamer space structures. This is mainly due to the fact that the membrane structures can be made exceptionally low in mass and packaged into very small volumes [Jenkins (2001)]. Typical space membranes consist of a very thin load-bearing layer with metallic coating layers for reflection and thermal control. While these were widely considered as isotropic, there can be some sources of anisotropy resulting from packaging creases or the way the membranes are manufactured. The thin membranes have zero or very small bending rigidity and are buckled almost immediately under compression, which is called wrinkling. The wrinkling, along with the inherently large deformation accompanied during loading, makes the analysis of membrane structures a challenging task.

Recently, a number of numerical analyses have been performed to study wrinkling. The wrinkling algorithms employed in these studies can be categorized into two approaches: deformation tensor modification [Roddeman, Drukker, and Oomens (1987a and 1987b); Roddeman (1991); Kang and Im (1997); Lu, Accorsi, and Leonard (2001); Nakashino and Natori, (2003)] and stiffness/compliance modification [Miller, Hedgepeth, Weingarten, and Das (1985); Miyazaki and Nakamura (1998); Liu, Jenkins, and Schur (2000 and 2001)]. While the former approach provides rigorous mathematical formulation of the wrinkling mechanism, the latter is physically motivated and much simpler, and can be easily implemented to existing finite element codes for the analysis of isotropic membrane structures with wrinkles. Detailed wrinkled shapes were predicted by other researchers, where geometrically non-linear post-buckling analyses were performed for rectangular solar sail membranes with refined shell element meshes seeded with a random [Tessler, Sleight, and Wang (2003)], or a combination of selected bifurcation eigenmodes [Wong, Pellegrino, and Park (2003); Su, Abdi, Taleghani, and Blandino (2003)], geometrical imperfections to instigate out-of-plane wrinkling deformation. In these analyses, high mesh refinement was necessary to represent high spatial frequency wrinkle deformation reasonably, as well as to avoid element locking. Lee, Cho and Lee (2002) developed a specially formulated shell element to alleviate the locking problem for thin shells. The bulk of the above referenced works has been concerned only with the isotropic membrane case.

There are several reasons to motivate the analysis of anisotropic membranes, however. Most real membrane structures are fabricated from thin polymer sheets, many of which have oriented polymer chains due to the manufacturing process (*e.g.*, calendaring); often this orientation is referred to as the “machine” and “transverse” directions. Even in cases where the sheets may be initially isotropic, creases resulting from handling and packaging, and seams required to fabricate large areas, can all lead to an “effective anisotropy”. Analysis of wrinkling in

[1] Structural Systems & CAE Department, Chungbuk National University, Cheongju, Chungbuk, 361-763, Korea
[2] Institute of Space Technology and Aeronautics, Japan Aerospace Exploration Agency, Chofu-city, Tokyo, 181-8522, Japan
[3] Mechanical Engineering Department, South Dakota School of Mines & Technology, Rapid City, SD 57701, U.S.A

anisotropic membranes presents special challenges that will be subsequently discussed.

In this study, a membrane wrinkle analysis procedure was developed for anisotropic membranes. The procedure consists of a penalty-parameter modified material (*PPMM*) model and a non-linear root finding to simulate the uni-axial stress state. The algorithm was implemented in the ABAQUS finite element code as a user subroutine. In the following, the procedure is described in detail. Next, it is applied to partly wrinkled anisotropic annular and square membranes (that may be, for example, considered as prototypes of solar sail membranes). The same wrinkle problems are also solved by shell element post-buckling analysis and the results are compared. Lastly, the effect of anisotropy and unsymmetric loading on the wrinkling behavior is investigated.

2 Description of wrinkling model

The basic principle of the penalty-parameter based wrinkling algorithm is to numerically simulate the uni-axial stress state for wrinkled membranes by modifying the constitutive relation [Liu, Jenkins, and Schur (2000, 2001)].

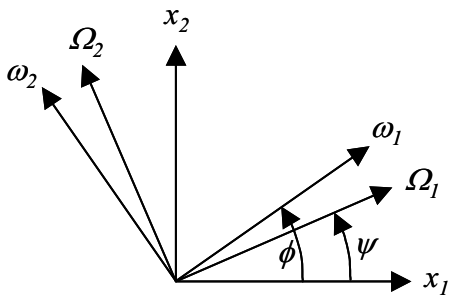

Figure 1 : Definition of element (x_1, x_2), principal (Ω_1, Ω_2), and wrinkle coordinate systems (ω_1, ω_2).

Consider an isotropic membrane element where stresses/strains are given for the unwrinkled configuration. Fig. 1 shows coordinate systems: element coordinate system (x_1,x_2) where the material properties are defined, principal stress coordinate system (Ω_1,Ω_2), and wrinkle coordinate system (ω_1,ω_2). The wrinkle coordinate system is defined in such a way that, when wrinkles occur in an element, the element is in a uni-axial stress state in the ω_2-direction. The angles ψ and ϕ define the positive rotations from the element coordinates to the principal and the wrinkle coordinates, respectively. The principal stresses and direction are calculated as

$$\sigma_{\min} = \frac{\sigma_{11}+\sigma_{22}}{2} - \sqrt{\left(\frac{\sigma_{11}-\sigma_{22}}{2}\right)^2 + \sigma_{12}^2}$$

$$\sigma_{maj} = \frac{\sigma_{11}+\sigma_{22}}{2} + \sqrt{\left(\frac{\sigma_{11}-\sigma_{22}}{2}\right)^2 + \sigma_{12}^2}$$

$$\psi = \tan^{-1}\frac{\sigma_{12}}{\sigma_{\min}-\sigma_{11}} \tag{1}$$

The stress-strain relationship in the principal coordinates is written as

$$\begin{Bmatrix} \sigma_{\min} \\ \sigma_{maj} \\ 0 \end{Bmatrix} = \begin{bmatrix} D_{11} & D_{12} & 0 \\ D_{12} & D_{22} & 0 \\ 0 & 0 & D_{33} \end{bmatrix} \begin{Bmatrix} \varepsilon_{\min} \\ \varepsilon_{maj} \\ 0 \end{Bmatrix} \tag{2a}$$

or

$$\begin{Bmatrix} \varepsilon_{\min} \\ \varepsilon_{maj} \\ 0 \end{Bmatrix} = \begin{bmatrix} S_{11} & S_{12} & 0 \\ S_{12} & S_{22} & 0 \\ 0 & 0 & S_{33} \end{bmatrix} \begin{Bmatrix} \sigma_{\min} \\ \sigma_{maj} \\ 0 \end{Bmatrix} \tag{2b}$$

The principal stresses and strains are used to determine whether the element is taut, wrinkled, or slack. This can be done by applying the mixed criterion [Kang and Im, (1997)] where

$$\begin{aligned} &\text{(i)} \quad \text{if } \sigma_{maj} > 0 \quad \Rightarrow \text{taut,} \\ &\text{(ii)} \quad \text{if } \sigma_{\min} \le 0 \text{ and } \varepsilon_{maj} > 0 \quad \Rightarrow \text{wrinkled,} \\ &\text{(iii)} \quad \text{if } \varepsilon_{maj} \le 0 \quad \Rightarrow \text{slack.} \end{aligned} \tag{3}$$

If the membrane is taut, no modification is necessary in the stress-strain relation. If it is slack, all stiffness components are reduced to near zero values (*i.e.*, $D^*_{ij} = D_{ij}/P$, where P is a penalty number). If it is wrinkled, wrinkling occurs in the principal coordinate directions where the shear stress is zero. Thus, the principal and wrinkle coordinate systems coincide for isotropic materials, *i.e.*, $\phi = \psi$. To eliminate the minor principal stress and thus have the uni-axial stress state, the S_{11} of the compliance matrix is penalized to PS_{11} in the principal coordinate system, where P is the large penalty number. The resulting modified stress-strain relations are written as

$$\begin{Bmatrix} \sigma^*_{\min} \\ \sigma^*_{maj} \\ 0 \end{Bmatrix} = \begin{bmatrix} D^*_{11} & D^*_{12} & 0 \\ D^*_{12} & D^*_{22} & 0 \\ 0 & 0 & D_{33} \end{bmatrix} \begin{Bmatrix} \varepsilon_{\min} \\ \varepsilon_{maj} \\ 0 \end{Bmatrix} \tag{4}$$

where

$$D^*_{11} = \frac{S_{22}}{PS_{11}S_{22} - S_{12}S_{12}} \to 0$$
$$D^*_{22} = \frac{PS_{11}}{PS_{11}S_{22} - S_{12}S_{12}} \to \frac{1}{S_{22}}$$
$$D^*_{12} = \frac{-S_{12}}{PS_{11}S_{22} - S_{12}S_{12}} \to 0 \qquad (5)$$

Here the superscript * was used to denote variables modified by the penalization. From Eqs.4 and 5, one can see that $\sigma^*_{\min}$ vanishes and, thus, the uni-axial stress state has been achieved with σ^*_{maj} in the ω_2-direction. The modified stress and stiffness in the principal coordinate system are then transformed to the element coordinate system, which are used to calculate the new element stiffness matrix and force vector.

It should be noted that the vanishing of a diagonal term in the tangent stiffness is troublesome since in that case the stiffness matrix can be singular. To avoid this numerical problem, the size of the penalty number (P) is controlled to provide the necessary stiffness but small enough not to affect the final solution.

In the case of *anisotropic* membranes, the wrinkling does not necessarily occur in the principal directions. Since there is coupling between the normal and shear stress/strain components, the [D] and [S] matrices are fully populated. Penalizing $S_{11} \to PS_{11}$ to eliminate the minor principal stress in the principal stress coordinates would result in non-zero shear stress values and thus the uni-axial stress condition is not achieved. This can be illustrated from a simple example. Fig. 2 shows the stress/strain variation versus coordinate system rotation angle (θ) for a given orthotropic material properties and strain state. The unwrinkled principal stress direction occurs at θ = 0.831 rad where σ_{22} is maximum with zero σ_{12}. However, after penalization to eliminate σ_{11}, the shear stress becomes non-zero in this direction and it does not become the uni-axial stress state. Instead, the shear stress vanishes at a slightly different direction of $\theta = 0.653$ rad as shown in Fig. 2(b) which is the correct wrinkle direction. (σ_{22} is maximum in this case at $\theta =$ 0.888 rad.)

The wrinkling direction for the anisotropic membranes can be found by a combination of the penalization and a root-finding procedure. Assume that the wrinkling occurs in a coordinate direction (ω_1,ω_2) rotated by ϕ from the element coordinates (x_1,x_2). (Superscripts tilde are used to denote variables in the wrinkle coordinates.) To test whether this is the correct wrinkling direction, the following steps are performed.

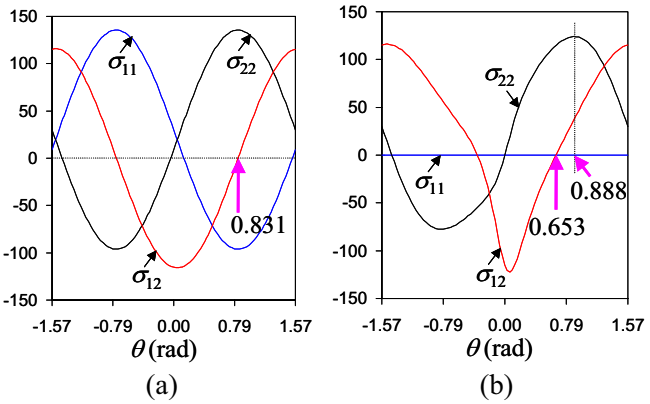

Figure 2 : Variation of stresses versus coordinate system rotation angle for an orthotropic membrane: (a) unpenalized, and (b) penalized. Elastic constants and strains are given as $E_{11} = 10^5$Pa, $E_{22} = 10^6$ Pa, $\nu_{12} = 0.03$, $G_{12} = 0.385x10^5$ Pa, $\varepsilon_{11} = 0.0003$, $\varepsilon_{22} = 0$, and $\gamma_{12} = -0.0003$.

- *Step 1:* Calculate $\{\tilde{\varepsilon}(\phi)\}$ and $[\tilde{S}(\phi)]$ by transformation.

- *Step 2:* Penalize $\tilde{S}_{11} \to P\tilde{S}_{11}$ and compute $[\tilde{D}^*(\phi,P)]$ and $\{\tilde{\sigma}^*(\phi,P)\}$.

- *Step 3:* Check if the following conditions are satisfied.

$$\tilde{\sigma}^*_{12}(\phi,P) = \tilde{D}^*_{23}(\phi,P)\tilde{\varepsilon}_{22}(\phi,P) + \tilde{D}^*_{33}(\phi,P)\tilde{\gamma}_{12}(\phi,P) = 0$$

$$\tilde{\sigma}^*_{22}(\phi,P) = \tilde{D}^*_{22}(\phi,P)\tilde{\varepsilon}_{22}(\phi,P) + \tilde{D}^*_{23}(\phi,P)\tilde{\gamma}_{12}(\phi,P) > 0 \qquad (6)$$

If the two conditions in *Step 3* are satisfied simultaneously, the current ϕ is the wrinkling direction and the modified stiffness and stress are back-transformed to the element coordinates. If not, *Steps 1-3* are repeated.

3 Numerical results

3.1 Annular membrane

The wrinkling algorithm developed in this study was first applied for verification to Mikulas' annulus membrane [Mikulas (1964)] and Stein and Hedgepeth's rectangular membrane [Stein and Hegepeth (1961)] with isotropic properties. It was found that the present algorithm was able to predict the wrinkling behavior accurately. The results of this verification were explained in detail in a separate paper (see Hossain, Jenkins, Woo, and Igawa (2004)] and thus not included herein.

To further verify the wrinkling algorithm for anisotropic properties, Roddeman's annular membrane problem was considered [Roddeman (1991)], in which the annular membrane is attached to a rigid disk at the inner hub and to a boundary ring at the outer edge. The inner radius of the membrane is 5 *m* and the outer radius 12.5 *m*. The material properties used are:

$$E_{11} = 10^5\,\text{Pa}, \quad E_{22} = 10^6\,\text{Pa}, \quad \nu_{21} = 0.3,$$
$$G = 0.385x10^5\,\text{Pa} \tag{7}$$

The problem was solved by geometrically non-linear membrane analysis with the present wrinkle algorithm and by shell element post-buckling analysis, both using ABAQUS. The meshes were modeled with M3D4 elements with wrinkle algorithm for the membrane analysis and S4 elements for shell analysis. In the shell analysis, a random geometrical imperfection with the magnitude of 0.1% of the thickness was applied to instigate the out-of-plane deformation, and *STATIC, STABILIZE option was used to stabilize the solution procedure with the default value of damping parameter in ABAQUS. The thickness of the membrane was 0.01 *m*. This thickness was selected for numerical purposes in which a small thickness was necessary for shell element analysis for the buckling to occur at a relatively lower load level, while too small a thickness could cause severe convergence problems from the large differences between the membrane and bending stiffnesses. In the analysis, the rigid inner hub was subjected to a 5^o rotation. The amount of the rotation was selected also for numerical purposes to limit the extensive computation time for the shell post-buckling analysis. The applied boundary conditions were such that all degrees of freedom were fixed at the outer hub, and the in-plane displacements for the rigid rotation were specified at the inner hub. In the shell analysis, the out-of-plane displacement and the rotations were also fixed at the inner hub.

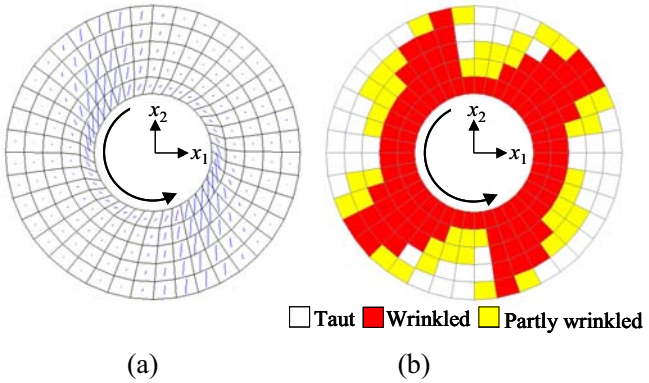

Figure 3 : Prediction of wrinkle shape by membrane analysis subjected to a rigid torque at the inner hub (NE=200): (a) tensile stress vector, and (b) wrinkled elements.

Fig. 3(a) shows the deformed mesh with direction of the major principal stress by the membrane analysis with a coarse mesh. The length of the line indicates the relative magnitude of the stress. Due to the anisotropy, a skewed stress distribution was found which agreed well with the result by Lu, Accorsi, and Leonard (2001). Shown in Fig. 3(b) is the predicted wrinkled region by the criterion given in Eq.3. Here, an element is denoted as wrinkled when wrinkling occurs for all integration points of the element, and partly wrinkled when wrinkling occurs for at least one integration point but not all. When all integration points are taut, the element is denoted as taut. The figure shows that wrinkling occurred in a cyclic pattern which agrees well with that of the experimental result by Miyamura (2000). It can be seen that all the elements near the inner hub where the rigid rotation was applied were wrinkled, while the cyclic partial wrinkling occurred at the outer region.

This wrinkling pattern can be understood considering the stress distribution. Figs. 4 and 5 show the distribution of the *initial unwrinkled* and *final wrinkled* major and minor principal stresses, respectively. The arrows indicate the region where the maximum stresses were occurred. Note that while there was little change between the initial and final major stress distributions, the initially all negative minor principal stresses became positive in the final distribution, and the region with near zero minor principal

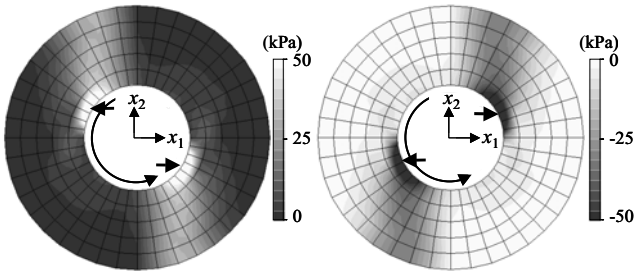

Figure 4 : Distribution of *unwrinkled* principal stresses: (a) σ_{maj} and (b) σ_{min}. The arrows indicate stress concentration points.

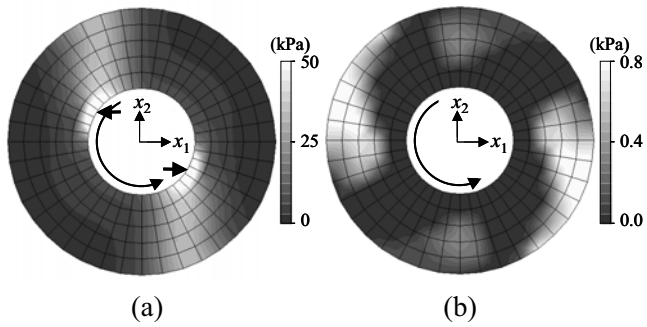

Figure 5 : Distribution of *wrinkled* principal stresses: (a) σ_{maj} and (b) σ_{min}. The arrows indicate stress concentration points.

stresses in Fig. 5(b) coincides with the wrinkled region in Fig. 3(b). Comparing the wrinkle shape with the stress distribution, one can see that there occurred two tension wrinkles at θ=117^o and -63^o, and two compression wrinkles at θ=36^o and -144^o, approximately. The wrinkling was thought to initiate at the stress concentrated region at the inner hub indicated by arrows in Fig. 4, and then proceed to the outer hub.

For comparison of membrane and shell analysis results, a series of mesh convergence tests were performed. The considered mesh sizes were varied to model the annulus with from 200 to 20,000 elements. Fig. 6 shows the variation of the maximum tensile stress (σ_{max}) and the tensile stress at an arbitrary point x_o (σ_{xo}) versus the number of elements. The maximum tensile stress occurred at two points of the inner hub rotated approximately by 150^o and -30^o from the x_1-axis. The point x_o, located at a mid point in the wrinkled region (r=8.75m, θ=117^o), was selected only for comparison purposes. As can be seen in the figure, the tensile stress σ_{xo} by both the membrane and shell analyses converged quickly as the number of elements increased. Compared respectively to the σ_{xo}'s calculated using 20,000 element meshes, 3,200 membrane elements and 7,400 shell elements produced the converged results with less than 1% differences. In addition, the σ_{xo}'s by the membrane and shell analyses agreed well to each other. The difference in σ_{xo} was 1.7% when 20,000 elements were used. In the case of the maximum tensile stress, the membrane analysis also showed a good convergence. The σ_{max} with 3,200 elements was different only by 1.2% from that with 20,000 elements. However, the convergence by the shell analysis was much slower for the σ_{max}. When using 20,000 elements, the shell analysis underestimated the σ_{max} by 7.0% compared to the membrane result.

Fig. 7 compares the predicted wrinkled region by the membrane element analysis with the out-of-plane deformation shape by the shell element post-buckling analysis. The plotted results were obtained by 3,200 membrane elements and 20,000 shell elements. The figure shows that the membrane element wrinkled region agreed well with the region having the non-zero out-of-plane displacements by the shell analysis, although it was difficult to specify the exact wrinkle boundary from the shell element deformed shape. While the shell analysis was able to provide more visual wrinkle information including crests and troughs, it required a much higher mesh density to capture the detailed post-buckled wrinkle pattern. For the shell models considered in this study, a reasonable wrinkle deformation was obtained only when more than 12,800 elements were used.

To investigate the effect of anisotropy on wrinkling, analyses were performed for the annular membrane with various properties. While keeping the values shown in Eq.6 for E_{11}, ν_{21}, and G_{12}, the values in the range of 1 to 15 times E_{11} were considered for E_{22}, *i.e.*, E_{22}/E_{11}=1$\sim$15, with E_{22}/E_{11}=1 being isotropic. The calculations were performed using the present wrinkling algorithm with 3,200 membrane elements. Fig. 8 shows the wrinkled shape versus the anisotropic modulus ratio (E_{22}/E_{11}). As expected, a circumferentially uniform wrinkled shape occurred when the isotropic properties were used (E_{22}/E_{11}=1). Note that a strip region at the outer boundary was unwrinkled (a 3 element strip was taut bounded by a partly wrinkled 1 element strip), while

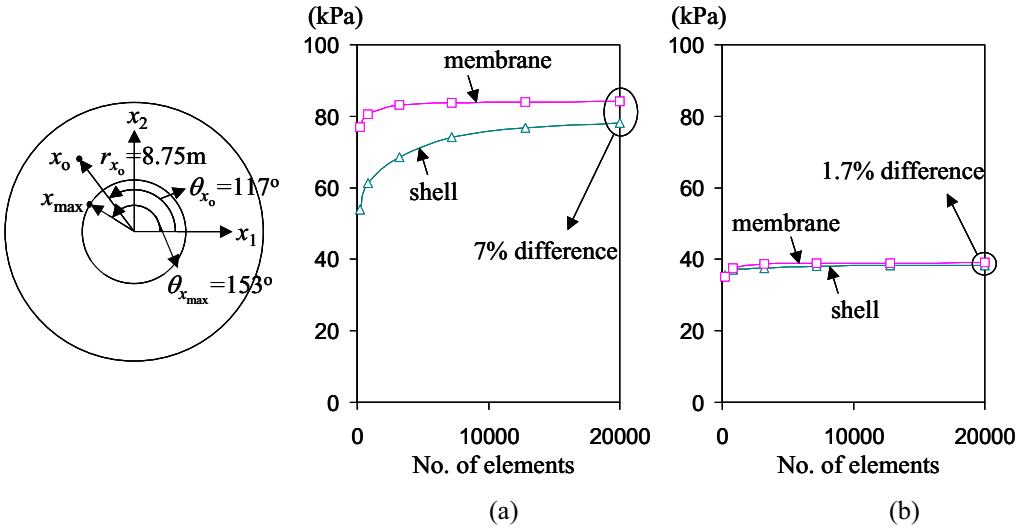

Figure 6 : Convergence of tensile stress versus number of elements: (a) σ_{max}, and (b) σ_{x_o}. σ_{max} is the maximum tensile stress achieved at point x_{max} indicated by arrows in Figure 5(a), and σ_{x_o} the tensile stress at point $x_o (r_{x_{max}} = 5m, \theta_{x_{max}} = 153^o, r_{x_o} = 8.75m$, and $\theta_{x_o} = 117^o)$.

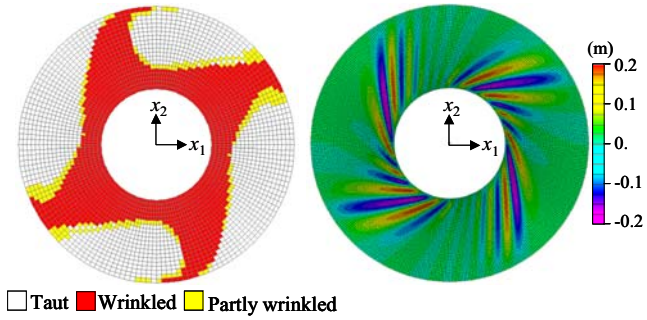

Figure 7 : Comparison of wrinkle shape: (a) membrane wrinkled elements (*NE*=3,200), and (b) distribution of shell out-of-plane displacement (*NE*=20,000).

a linear elastic solution without wrinkling algorithm predicted full wrinkling where the whole membrane region wrinkled immediately after applying the rigid rotation. The unwrinkled strip is due to the induced stretching near the outer region, which gives the effect of a radial tension applied at the outer boundary and, thus, results in the partial wrinkling [Miller, Hedgepeth, Weingarten, and Das (1985)]. As the anisotropy ratio increased, the wrinkling pattern became uneven and gradually narrowed. It can be seen that the two upper left and lower right wrinkle bands coincided to the higher tensile stress region shown in Fig. 5(a). The other wrinkle bands were thought to initiate at the compressive stress concentrated region of the inner hub indicated by the arrows in Fig. 4(b), and propagate in the radial direction. Fig. 9 shows the variation of percent wrinkled area versus the anisotropy ratio. For the isotropic properties, 77.9% of the membrane was wrinkled, which was reduced as the anisotropy ratio increased. When E_{22}/E_{11}=15, the wrinkle area was 43%.

3.2 Square membrane

Fig. 10 shows a 500 mm square membrane loaded at the corners through cables. The thickness is 0.0254 mm. To apply the load, the corners are cut-off with the edge length of 14 mm and connected at the edge center to 1 mm radius cables with the elastic modulus of 70.3 GPa. The length of the cables is 57 mm. The material properties considered for the membrane are shown in Tab. 1. The anisotropic modulus ratio (E_{22}/E_{11}) is 0.67 and 0.2 for the low and high anisotropic membranes, respectively. The positive material coordinate orientation angle (θ) is defined as the counter-clock-wise rotation from the global x_1-axis.

The membrane was modeled with 10,000 membrane elements (M3D4/M3D3) with wrinkle algorithm, and the cables with rod elements (T3D2). Rigid bar elements were added to the cut-off edges to distribute the applied load. Analyses were also performed for comparison us-

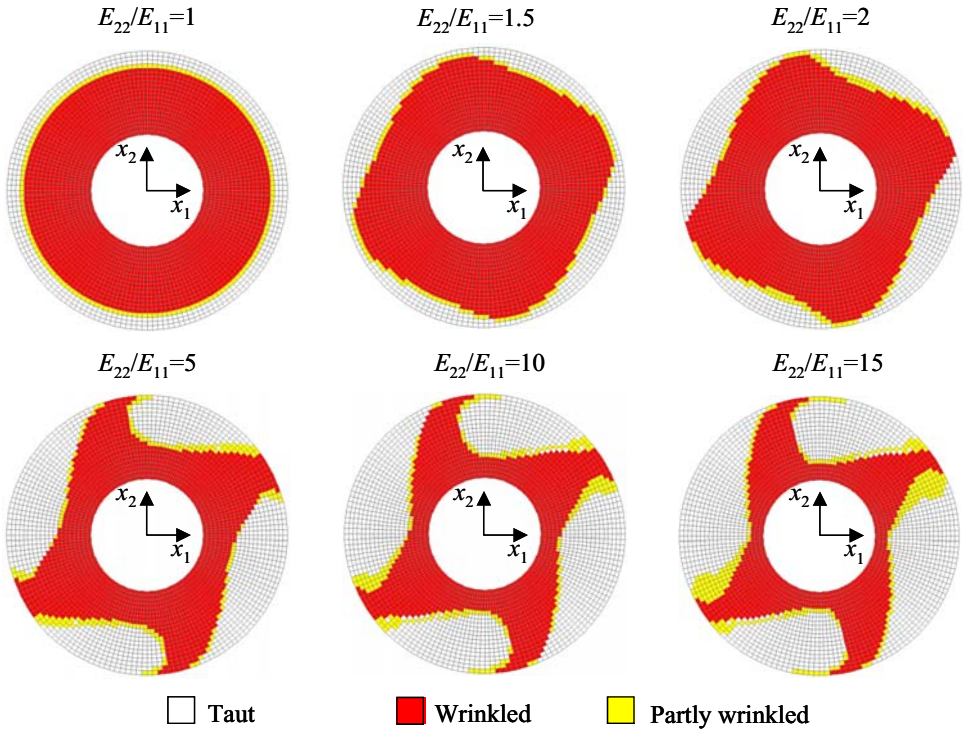

Figure 8 : Variation of wrinkled shape versus anisotropy ratio (E_{22}/E_{11}).

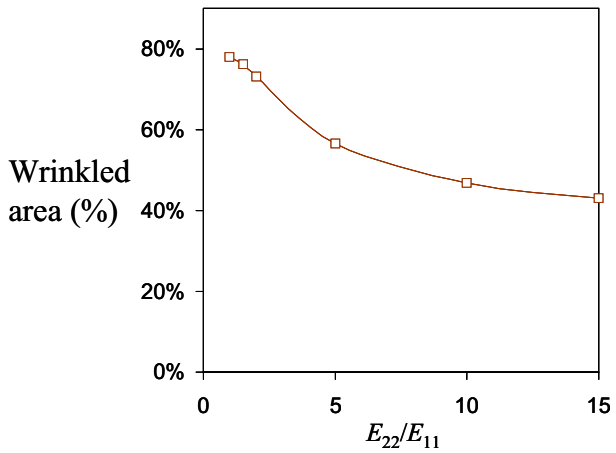

Figure 9 : Percent wrinkled area versus anisotropy ratio.

ing 19,208 shell elements (S4R5/S3R) with a random initial geometrical imperfection (applied at the interior region of the membrane) and *STATIC, STABILZE option. Loading was applied in such a way that $T_1 = T_2$=0.49N was applied symmetrically in the first load step, and then T_2 was increased up to 1.96N while T_1 remained at 0.49N in the second step.

Table 1 : Elastic properties considered for square solar sail membrane.

	E_{11} (GPa)	E_{22} (GPa)	ν_{12}	G_{12} (GPa)
Low anisotropic	2.59	1.727	0.34	0.704
High anisotropic	2.59	0.518	0.34	0.243
Isotropic	2.59	–	0.34	–

Figs. 11 and 12 compare the tip displacement history and the wrinkle shapes versus the load ratio for the case when E_{22}/E_{11}=0.67 and the orientation angle θ=0 ^{o}. Good agreements were obtained between the results by the membrane element and shell element analyses. The agreement was better for d_2 in the direction where the higher load T_2 was applied. The figure shows that the displacements varied almost linearly at the beginning, and then the variation changed abruptly as the load ratio increased. The abrupt curving of the variation trend in the tip displacements is due to the forming of the global wrinkles from small local corner wrinkles. As can be seen in Fig. 12, only the areas near the corners were

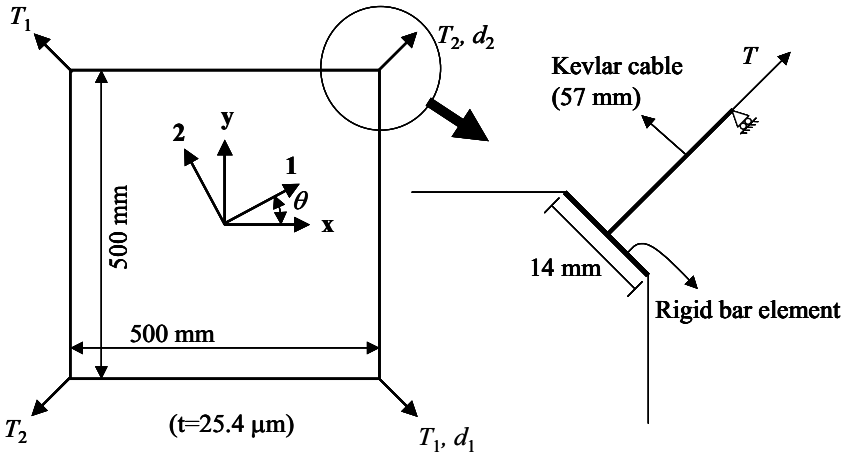

Figure 10 : Corner-loaded square membrane.

wrinkled when T_2/T_1=1 and the rest of the membrane was in the taut state. When the load ratio was increased to T_2/T_1=2, the wrinkled region grew at the T_2 corners where the higher load was applied. As the load ratio continued to increase, the local wrinkles at the T_2 corners merged into global wrinkles at about T_2/T_1=2.6, which approximately coincided to the curving point. In Fig. 12, the wrinkled shape for T_2/T_1=3 clearly shows the global wrinkles were formed. Note that the curving point occurred slightly later for the shell element analysis. This was expected and thought to be due to the small bending stiffness the shell elements had, which resisted the snapping merge of the wrinkle.

Fig. 13 shows the variation of the wrinkled region versus orientation angle predicted by the membrane analysis for E_{22}/E_{11}=0.67 and 0.2 when the load was applied symmetrically, *i.e.*, T_2/T_1=1. As can be seen in the figure, for both membrane properties the wrinkling occurred mostly near the corners where the load was applied, with the much larger area wrinkled for the higher anisotropic case of E_{22}/E_{11}=0.2. As the material orientation angle changed, the wrinkling pattern was consistently following the material axis, in which the taut region tended to align with the major material direction and more wrinkling occurred near the corners in the minor material direction. The variation of the wrinkled region when T_2/T_1=3 is plotted in Fig. 14. In this case, the wrinkle pattern was dominated by the global wrinkling due to the high load ratio. The wrinkle shapes were again strongly dependant on the orientation angles for both cases of anisotropy ratios, however, the effect was more apparent

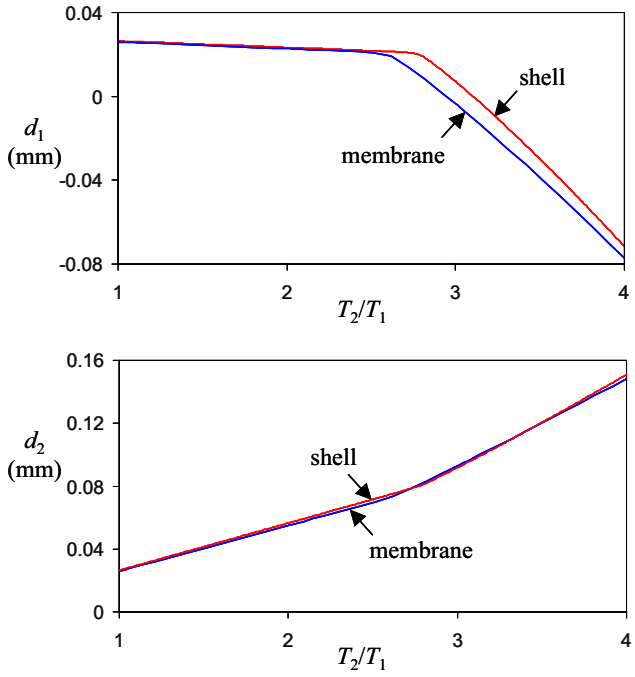

Figure 11 : Comparison of corner displacements.

for the higher anisotropic case.

The variation of percent wrinkled area is plotted in Fig. 15 versus the orientation angle. The results for the isotropic membrane are also indicated for comparison. The figure shows that the maximum wrinkling occurred for all cases at $\theta = -45^{o}$, where the minor material direction coincided with the higher load application direction. However, the minimum wrinkling occurred at different

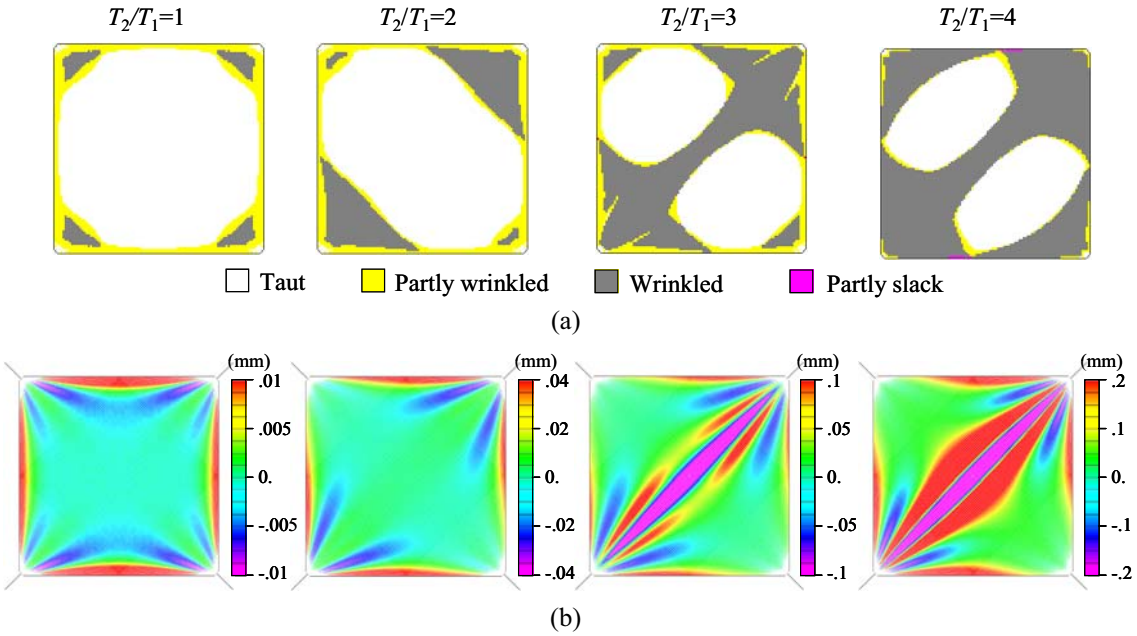

Figure 12 : Wrinkled shape of sail membrane: (a) membrane analysis, and (b) shell post-buckling analysis.

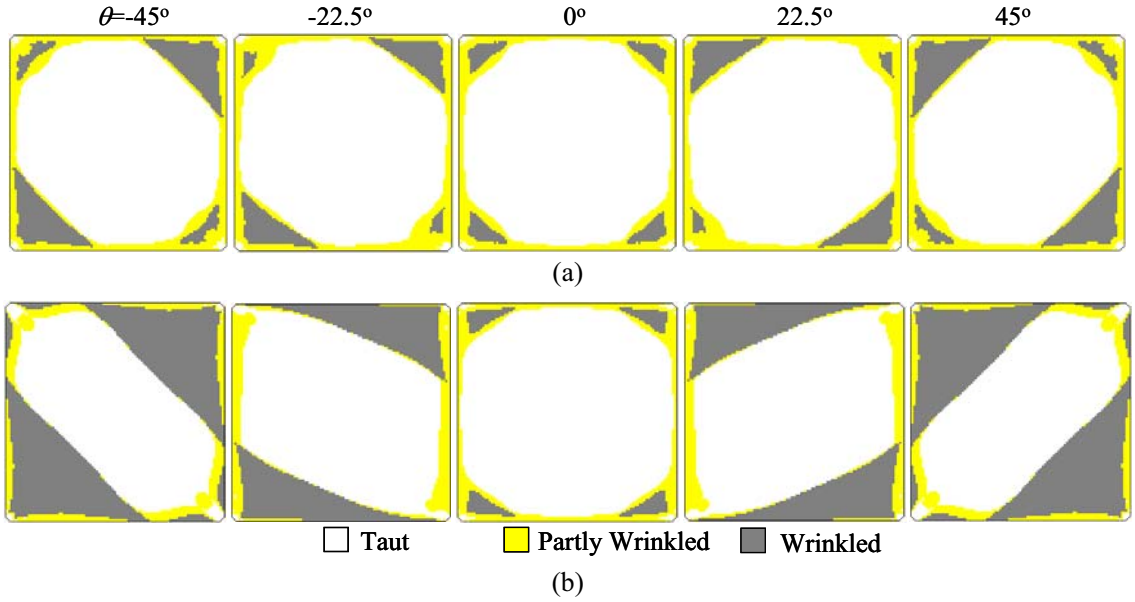

Figure 13 : Comparison of wrinkled shapes for $T_2/T_1 = 1$: (a) $E_{22}/E_{11} = 0.67$, and (b) $E_{22}/E_{11} = 0.2$.

orientation angles depending on the load ratios (T_2/T_1) and the anisotropy ratios (E_{22}/E_{11}). When T_2/T_1=1 and 2, the minimum wrinkling orientation angle was 0 ° regardless of the anisotropy ratio, where the minor material axis was aligned away from either corners where the loads were applied and where most local wrinkles were concentrated. In contrast, when T_2/T_1=4 the high load ratio had dominating effect with global wrinkles, and the minimum wrinkling occurred at θ=45 ° where the major material axis oriented with the higher load direction. When T_2/T_1=3, the minimum wrinkling occurred at the intermediate angle of θ=22.5 ° for E_{22}/E_{11}=0.67,

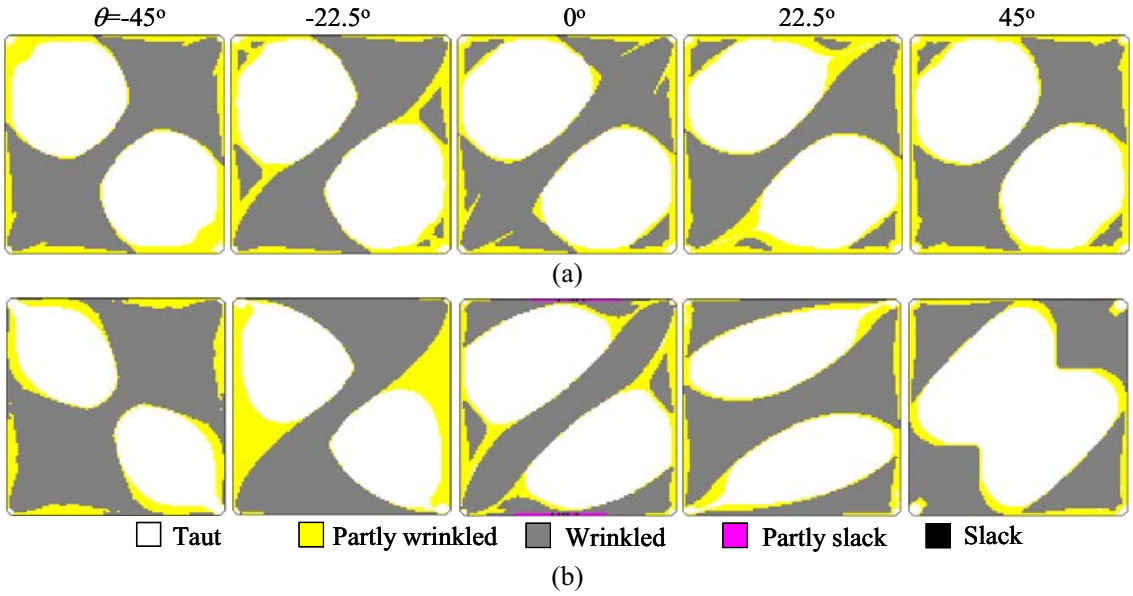

Figure 14 : Comparison of wrinkled shapes for $T_2/T_1 = 3$: (a) $E_{22}/E_{11} = 0.67$, and (b) $E_{22}/E_{11} = 0.2$.

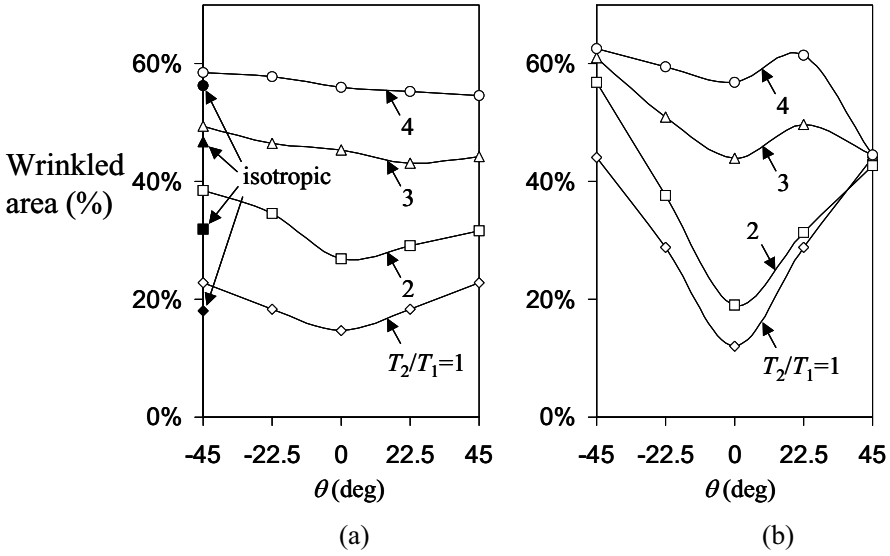

Figure 15 : Variation of % wrinkled area versus orientation angle: (a) $E_{22}/E_{11} = 0.67$, and (b) $E_{22}/E_{11} = 0.2$.

while it occurred still at θ=0° for E_{22}/E_{11}=0.2. In the latter case, the % wrinkled area had local peaks between θ=0° and 45° for T_2/T_1=3 and 4, which was thought to be due to the interplay of the higher load and anisotropy ratios. It was also found that the amount of the wrinkled area showed higher dependency on the anisotropy ratio as the orientation angle changed when the load ratio was smaller. Compared to the isotropic membrane results, when T_2/T_1=1 the maximum wrinkled area was increased by 26.5% for E_{22}/E_{11}=0.67, and significantly (by 145%) for E_{22}/E_{11}=0.2. The dependency reduced for the higher load ratio cases. When T_2/T_1=4, the maximum difference was 4.1% for E_{22}/E_{11}=0.67, and 11.1% for E_{22}/E_{11}=0.2. When the high anisotropy properties (E_{22}/E_{11}=0.2) were used, a small portion of the membrane became slack depending on the orientation angle. As the slack area started to develop, the analysis suffered a severe convergence problem due to the lack of diagonal stiffness terms

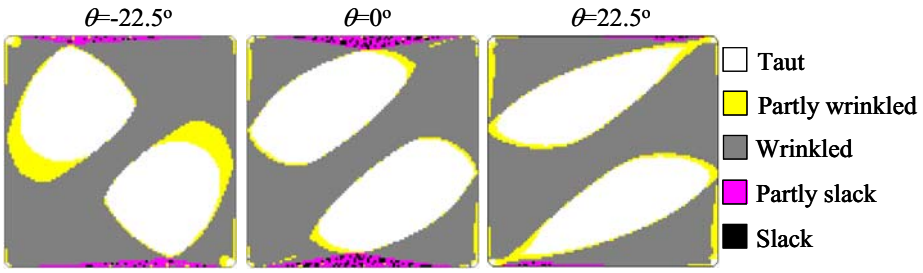

Figure 16 : Wrinkled/slack shape for the higher anisotropic membrane ($E_{22}/E_{11} = 0.2$) at $T_2/T_1 = 4$.

at the slack nodes. This resulted in large displacement corrections during iterations, though the residual forces were kept small. In this study, the *STATIC, STABILZE option was also used for the convergence in which a small amount of artificial damping was added that provided the needed resistance to the large displacement corrections. Fig. 16 shows the wrinkle/slack regions for θ=-22.5°, 0°, and 22.5° when T_2/T_1=4. The slack region occurred at and moved along the upper and lower free edges as the orientation angle changed. It started to appear at the load ratio of T_2/T_1=3.48 for θ=-22.5°, and much earlier at T_2/T_1=2.81 for θ=0°. The amount of slack area increased as the load ratio increased, and 1.78% for θ=-22.5° and 3.56% for θ=0° of the total membrane area became slack when the load ratio reached 4. The slack region also occurred for θ=22.5°, but only 0.64% was slack atT_2/T_1=4. For other orientation angles, no slack area was found for the considered load ranges.

4 Conclusion

In this study, a reliable finite element procedure was developed for the analysis of wrinkles for anisotropic membranes. The wrinkling algorithm was based on a penalty-parameter modified material model and a non-linear root finding, and was implemented as a user subroutine to the general finite element analysis code ABAQUS. The procedure was first used to solve isotropic membrane wrinkle problems with known solutions and then applied to anisotropic annular and square membranes. The latter membrane problems were also solved by shell element post-buckling analysis with random geometrical imperfection and the results were compared. It was found that the present wrinkle algorithm produced accurate wrinkle results compared to those published in the literature, and the wrinkled region predicted for the anisotropic membranes was in good agreement with that by the shell element post-buckling analysis, but with less computational cost. It was also found that both the material anisotropy and the load ratio had significant effect on the wrinkling behavior for the square membrane.

Acknowledgement: This work was supported by the 2003 Foreign Study Program of Chungbuk National University, and NASA. The financial support is gratefully acknowledged.

References

Adler, A.; Mikulas, M. M.; Hedgepeth, J. M. (2000): Static and Dynamic Analysis of Partially Wrinkled Membrane Structures. *Proc. 41st AIAA/ASME/ASCE/AHS SDM Conf.*, AIAA 2000-1810, Atlanta, GA.

Hossain, N. M. A.; Jenkins, C. H.; Woo, K.; Igawa, H. (2004): Penalty Parameter Material Model for Static and Dynamic Analysis of Partly Wrinkled Membranes. submitted to *Int. J. Numerical Methods in Engineering.*

Jenkins, C. H. (2001): Gossamer Spacecraft: Membrane and Inflatable Structures Technology for Space Applications, AIAA, Inc., Reston, Virginia.

Kang, S.; Im, S. (1997): Finite Element Analysis of Wrinkling Membranes. *J. Applied Mechanics*, vol. 64, pp. 263-269.

Lee, K.; Cho, C.; Lee, S. W. (2002): A Geometrically Nonlinear Nine-Node Solid Element Formulation with Reduced Sensitivity to Mesh Distortion. *CMES: Computer Modeling in Engineering & Science*, vol. 3, no. 2, pp. 339-349.

Liu, X.; Jenkins, C. H.; Schur, W. W. (2000): Fine Scale Analysis of Wrinkled Membranes. *Int. J. Computational Science*, vol. 1, no. 2, pp. 281-298.

Liu, X., Jenkins; C. H.; Schur, W. W. (2001): Large Deflection Analysis of Pneumatic Envelopes using a Penalty Parameter Modified Material Model. *Finite Elements in Analysis and Design*, vol. 37, pp. 223-251.

Lu, K.; Accorsi, M.; Leonard, J. (2001): Finite Element Analysis of Membrane Wrinkling. *Int. J. Numerical Methods in Engineering*, vol. 50, pp. 1017-1038.

Mikulas, M. M. (1964): Behavior of a Flat Stretched Membrane Wrinkled by the Rotation of an Attached Hub. *NASA TN D*-2456.

Miller, R. K; Hedgepeth, J. M.; Weingarten, V. I.; Das, P. (1985): Finite Element Analysis of Partly Wrinkled Membranes. *Computers and Structures*, vol. 20, pp. 631-639.

Miyamura, T. (2000): Wrinkling on Stretched Circular Membrane under In-plane Torsion: Bifurcation Analysis and Experiments. *Engineering Structures*, vol. 23, pp. 1407-1425.

Miyazaki, Y.; Nakamura, Y. (1998): Dynamic Analysis of Deployable Cable-Membrane Structures with Slackening Membrane. *Proc. 21st Int. Symp. on Space Technology and Science*, Omiya, Japan.

Nakashino, K.; Natori, M. C. (2003): Efficient Modification Scheme of Stress-Strain Tensor for Finite Element Analysis of Wrinkled Membranes. *Proc. 44th AIAA/ASME/ASCE/AHS SDM Conf.*, AIAA 2003-1981, Norfolk, Virginia.

Roddeman, D. G.; Drukker, J.; Oomens, C. W. J.; Janssen, J. D. (1987a): The Wrinkling of Thin Membranes: Part I – Theory. *J. Applied Mechanics*, vol. 54, pp. 884-887.

Roddeman, D. G.; Drukker, J.; Oomens, C. W. J.; Janssen, J. D. (1987b): The Wrinkling of Thin Membranes: Part II - Numerical Analysis. *J. Applied Mechanics*, vol. 54, pp. 888-892.

Roddeman, D. G. (1991): Finite-Element Analysis of Wrinkling Membranes. *Communications in Applied Numerical Methods*, vol. 7, pp. 299-307.

Stein, M.; Hedgepeth, J. M. (1961): Analysis of Partly Wrinkled Membrane. *NASA TN D*-813.

Su, X.; Abdi, F.; Taleghani, B.; Blandino, J. (2003): Wrinkling Analysis of A Kapton Square Membrane under Tensile Loading. *Proc. 44th AIAA/ASME/ASCE/AHS SDM Conf.*, AIAA 2003-1981, Norfolk, Virginia.

Tessler, A.; Sleight, D. W.; Wang, J. T. (2003): Nonlinear Shell Modeling of Thin Membranes with Emphasis on Structural Wrinkling. *Proc. 44th AIAA/ASME/ASCE/AHS SDM Conf.*, AIAA 2003-1981, Norfolk, Virginia.

Wong, Y. W.; Pellegrino, S.; Park, K. C. (2003): Prediction of Wrinkle Amplitudes in Square Solar Sails. *Proc. 44th AIAA/ASME/ASCE/AHS SDM Conf.*, AIAA 2003-1981, Norfolk, Virginia.